32.0 ALGORITHMIC ANALYSES OF X-RADIOGRAPHY AND COMPUTED TOMOGRAPHY FOR MULTISCALE STRUCTURAL INVESTIGATIONS OF METALS (LEVERAGED)

C. Gus Becker (Mines)
Faculty: Amy Clarke (Mines)
Industrial Mentor: Michelle Espy (LANL)

This project initiated in Fall 2017 and is supported by Los Alamos National Laboratory (LANL). The research performed during this project will serve as the basis for a Ph.D. thesis program for C. Gus Becker.

32.1 Project Overview and Industrial Relevance

X-radiography allows for the imaging of materials in a non-destructive manner by observing x-rays transmitted through the material. This method can be used for post-mortem analysis, as well as in-situ imaging of microstructural development. For example, dynamic imaging of microstructural evolution during processing (e.g. casting or directional solidification) can further our understanding of the mechanisms driving microstructural development, improving predictive capabilities [32.1]. X-radiography can also be used to capture multiple images of a sample from different angles, which can be reconstructed and represented as a three-dimensional model. A reconconstruction of a metal sample created with additive manufacturing (AM) can be generated to reveal microstructural characteristics and internal defects. Reconstructions can also be created from four-dimensional microscopy (three spatial and one temporal dimension), in which images are collected from different angles of a time-evolving sample. These reconstructions are created using techniques like the Time-Interlaced Model-Based Iterative Reconstruction (TIMBIR) [32.2], which improves temporal resolution to capture microstructural evolution during processing.

Synchrotron x-ray sources can be used to obtain high-spatial resolution x-ray radiographs (on the order of 1 μm), however these images have small fields of view and require significant beam time at national user facilities. High-energy microfocus x-radiography has lower spatial resolutions, but increases the field of view significantly and can be performed in a laboratory. These laboratory instruments consist of a high-energy microfocus x-ray source, radiation shielding (typically a lead-lined cabinet housing the source), a scintillator to convert x-rays to visible light, and a camera/detector to collect the produced light. Tomographic data can be obtained when a rotation stage is included. Solidifiation experiments are often performed at synchrotron x-ray facilities like the Advanced Photon Source (APS) at Argonne National Laboratory (ANL), as well as in facilities with microfocus x-ray capabilities, including the non-destructive testing group (E-6, formerly AET-6) at LANL to study the microstructures and properties of materials. Many experiments have been performed by CANFSA faculty and students at Mines to study different aspects of alloy solidification, such as crystal growth and solute segregation [32.1], primary dendrite spacing and size [32.3], dendrite fragmentation [32.4], and the effect of different cooling rates on solidification [32.5].

When x-radiography and computed tomography are used for the non-destructive imaging of metals, sample thickness is a contsraint for high density alloys. X-rays at national user facilities (with energies of ~30 keV) can typically penetrate thin foils of material (~100 μm to ~1 mm) to image thin sections or small volumes to produce computed tomographic reconstructions [32.5]. These typically cannot be used to image thicker or larger samples, unless special high-energy beamlines are used with x-ray energies up to ~150 keV. High-energy microfocus x-ray imaging utilizes x-rays with energies of up to 250 keV and beyond, allowing sample thicknesses on the order of millimeters and larger fields-of-view on the order of centimeters. Proton radiography (pRad), in which 800 MeV energy protons are used as an incident radiation source at LANL's Los Alamos Neutron Science Center (LANSCE), allows for even larger sample sizes and the ability to probe materials with high atomic numbers. However, this comes at the cost of lower spatial resolution [32.1]. Proof-of-concept experiments of Transmission High-Energy Electron Microscopy (THEEM), in which extremely high-energy electrons (15 GeV) are transmitted through samples at the Stanford Linear Accelerator Center (SLAC) to achieve deeply penetrating electron radiography have also been demonstrated [32.6]. This method has yet to be optimized, but holds potential for dynamic studies of high atomic number (Z) materials. The goal of this project is to establish high-energy (~160 keV), microfocus x-ray imaging in a laboratory setting at Mines, achieving capabilities between those of

synchrotron x-ray facilities (i.e. ~1-2 µm spatial resolution and ~2 x 2 mm^2 fields-of-view) and pRad (~ 25 µm spatial resolution at best for the ×7 magnifier and ~17 x 17 mm^2 field-of-view, although note that the ×1 lens provides a 12 × 12 cm^2 field of view). The establishment of this system will enable new understanding of materials during/after processing through the reconstruction and image analysis of computed tomography.

32.2 Previous Work

Prior to the start of this project, in situ solidification of metals was studied using synchrotron x-ray imaging at the APS and using high-energy microfocus x-ray radiography systems in a laboratory setting at LANL, in collaboration with E-6. Through the course of this project, image processing methods have been created to process data from these experiments. Once processed, this data can be analyzed to capture phenomena like the multiscale solidification dynamics in metallic alloys and defects related to AM processes.

These image processing methods have evolved from their original concept. At the beginning of the project, modular ImageJ macros that take a directory of images from an experiment, perform some processing method, and output a directory of edited images. The processed images are saved as separate files to preserve the original, unedited images. The modular nature of these scripts allowed for processing steps to be adapted at different stages of the routines without reperforming the entire routine, however, large amounts of storage space were required to save the altered images after each processing step was performed. To circumvent the storage issue, the processing methods were adapated to Python, which allowed the code to eventually be stored and executed from within Jupyter Notebooks [32.7]. Each Notebook file consists of "cells" in which Python code is written and executed. The output of the code in one cell is shown directly below that cell, and more cells can be added below that cell and its output. The variables defined in each cell are stored and accessible by successive cells. Functions from external Python modules can be imported into the Notebook and executed. This means that an image can be loaded using the Python package scikit-image [32.8], shown using the Python package matplotlib [32.9], and accessed by later cells in the Notebook. Custom functions can even be grouped into a local module/package, at which point that package can be imported into the Notebook. Images loaded at the beginning of the Notebook can be altered by these functions in a step-by-step manner, processed images displayed and analyzed at each step, without saving mutliple iterarions of the processed images. By doing this all in the Notebook, the cells in which the function calls are made also act as a log of processing history, drastically increasing the reproducibility of the processing routines. On top of executing Python code, the Notebook cells can also contain formatted text to hold notes, links, or explanations. This makes the Notebook more readable, and therefore accessible and reproducible.

32.3 Recent Progress

Jupyter Notebooks have been developed to process radiography data of the solidification of an Al-9.68 at% Ag alloy (**Figure 32.1**). This experiment was captured with high-energy microfocus x-radiography with LANL's E-6 using the same experimental setup as previous synchrotron x-ray experiments. In the microfocus experiments, a rectangular section of a steel bar was removed to act as a window for the transmittance of x-rays. Microfocus x-ray radiography allows for a larger field-of-view than synchrotron x-ray radiography, so the experiment designed for synchrotron radiography takes place in only a fraction of the captured area of the microfocus system.

A publication [32.9] comparing the solidified structures formed in this experiment across different modes of analysis has been accepted for a special edition of the Journal of The Minerals, Metals, and Materials Society (JOM): Advances in Multi-modal Characterization of Structural Materials. This work compares the x-radiography intensity of solidification structures, made more clear through processing (**Figure 32.2**), with the composition of the structures as determined by energy dispersive spectroscopy (EDS) (**Figure 32.3**). A processed radiograph at the end of the solidification experiment is overlaid on a backscattered electron (BSE) image captured in a scanning electron microscope (SEM). The SEM is also used to perform the EDS, and one of the BSE images contains the overlay of the position of the EDS scan across the sample. The x-radiographic intensities along the same line are compared and show similar trends, even though the x-radiography is volume representation of the solidification structure while the EDS is only a surface representation (**Figure 32.4**).

The retrofitting of the high-energy microfocus x-ray cabinet donated from E-6 at LANL has been completed and the system has been delivered to the Mines campus. Installation of this system will begin October 19, 2021. This system will be used to perform a CT analysis of a variety of AM-built lattice structures for which CT has also been performed using the Zeiss Xradia 520 Versa Micro-CT located at Mines (**Figure 32.5a**). The datasets from the two different systems will allow for a comparison to be made between the techniques. 3D reconstructions from these CT analyses will also be compared to the build models (**Figure 32.5b**) used to create the structures to locate any defects. These defects will be evaluated to determine the defect detection limits of microfocus x-radiography.

Work has also resumed on automating the detection of the solid-liquid interface in the AM simulator experiments performed at the APS (**Figure 32.6**). The process currently requires a user to crop the image to a small region containing the melt pool. To make the process fully autonomous, focus is now moving towards improving the identificiation of the interface within the entire image.

32.4 Plans for Next Reporting Period

In the next reporting period, the following tasks will be completed:

- Improve level of automation of solid-liquid interface detection and adapt to Python Jupyter Notebooks for ease of reproducibility and presentation for publication.
- Adapt segmentation method combining intensity, edge, and shape information from literature to mock HE crystals (**Figure 32.7**).
- Perform CT analysis of AM-built lattice structures using the new high-energy microfocus x-ray cabinet and compare to data captured on the Zeiss Xradia Versa 520 Micro-CT instrument at Mines.

32.5 References

[32.1] P.J. Gibbs, S.D. Imhoff, C.L. Morris, F.E. Merrill, C.H. Wilde, P. Nedrow, F.G. Mariam, K. Fezzaa, W.K. Lee, A.J. Clarke, Multiscale X-ray and proton imaging of bismuth-tin solidification, JOM. 66 (2014) 1485–1492. https://doi.org/10.1007/s11837-014-1058-0.

[32.2] K.A. Mohan, S. V. Venkatakrishnan, J.W. Gibbs, E.B. Gulsoy, X. Xiao, M. De Graef, P.W. Voorhees, C.A. Bouman, TIMBIR: A Method for Time-Space Reconstruction From Interlaced Views, IEEE Trans. Comput. Imaging. 1 (2015) 96–111. https://doi.org/10.1109/TCI.2015.2431913.

[32.3] A.J. Clarke, D. Tourret, Y. Song, S.D. Imhoff, P.J. Gibbs, J.W. Gibbs, K. Fezzaa, A. Karma, Microstructure selection in thin-sample directional solidification of an Al-Cu alloy: In situ X-ray imaging and phase-field simulations, Acta Mater. 129 (2017) 203–216. https://doi.org/10.1016/j.actamat.2017.02.047.

[32.4] J.W. Gibbs, D. Tourret, P.J. Gibbs, S.D. Imhoff, M.J. Gibbs, B.A. Walker, K. Fezzaa, A.J. Clarke, In Situ X-Ray Observations of Dendritic Fragmentation During Directional Solidification of a Sn-Bi Alloy, JOM. 68 (2016) 170–177. https://doi.org/10.1007/s11837-015-1646-7.

[32.5] B.M. Patterson, K.C. Henderson, P.J. Gibbs, S.D. Imhoff, A.J. Clarke, Laboratory micro- and nanoscale X-ray tomographic investigation of Al-7 at.%Cu solidification structures, Mater. Charact. 95 (2014) 18–26. https://doi.org/10.1016/j.matchar.2014.06.004.

[32.6] F. Merrill, J. Goett, J. Gibbs, S. Imhoff, F. Mariam, C. Morris, L. Neukirch, J. Perry, D. Poulson, R. Simpson, P.L. Volegov, P.L. Walstrom, C. Hast, K. Jobe, T. Smith, U. Wienands, A.J. Clarke, D. Tourret, Demonstration of Transmission High Energy Electron Microscopy, (2017) 1–10.

[32.7] S. van der Walt, J.L. Schönberger, J. Nunez-Iglesias, F. Boulogne, J.D. Warner, N. Yager, E. Gouillart, T. Yu, scikit-image: image processing in Python, PeerJ. 2 (2014) e453. https://doi.org/10.7717/peerj.453.

[32.8] J.D. Hunter, Matplotlib: A 2D graphics environment, Comput. Sci. Eng. 9 (2007) 90–95. https://doi.org/10.1109/MCSE.2007.55.

[32.9] C.G. Becker, D. Tourret, D. Smith, B. Rodgers, S. Imhoff, J. Gibbs, J. Hunter, M. Espy, K. Clarke, A. Clarke, Integrating In Situ x-Ray Imaging, Energy Dispersive Spectroscopy, and Calculated Phase Diagram Analysis of Solute Segregation During Solidification of an Al-Ag Alloy, JOM. (2021). https://doi.org/10.1007/S11837-021-04884-8.

[32.10] C. Wälhby, I.M. Sintorn, F. Erlandsson, G. Borgefors, E. Bengtsson, Combining intensity, edge and shape information for 2D and 3D segmentation of cell nuclei in tissue sections, J. Microsc. 215 (2004) 67–76. https://doi.org/10.1111/J.0022-2720.2004.01338.X.

32.6 Figure and Tables

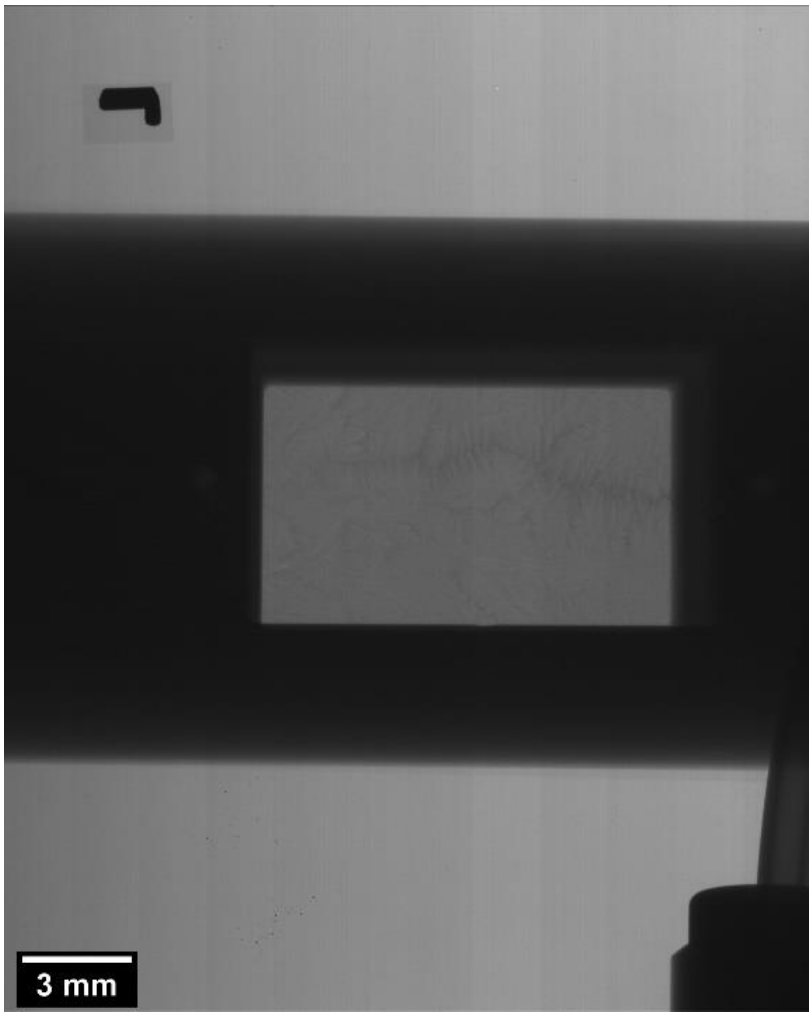

Figure 32.1: An unprocessed frame from the directional solidification of an Al- 9.68 at% Ag at.% alloy obtained using high-energy microfocus x-ray radiography of a sample undergoing directional solidification. The experiment was performed using the synchrotron x-radiography experimental setup, so the experiment is entirely contained in the small, light gray window in the center.

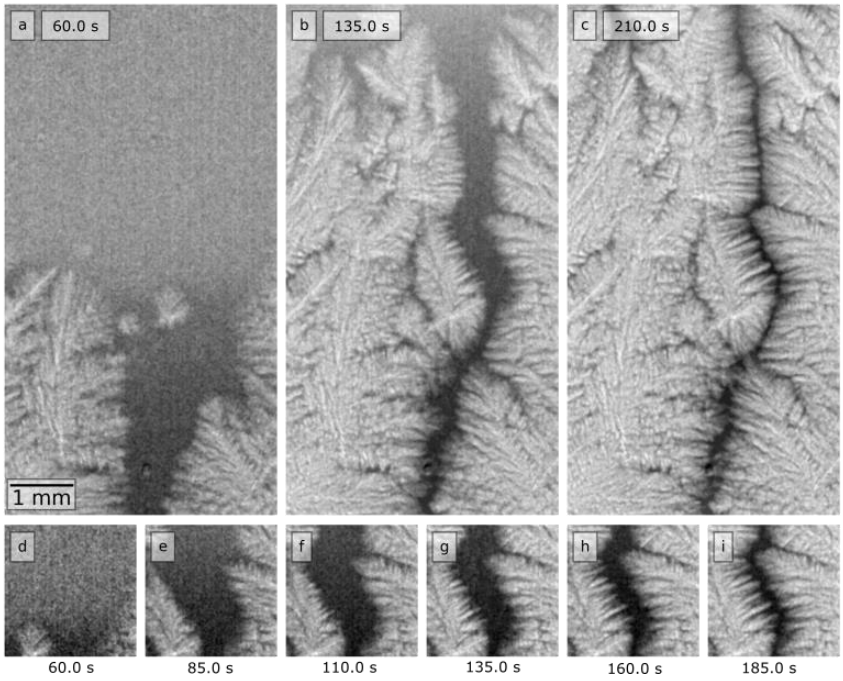

Figure 32.2: (a-c) In situ x-radiographs showing the mesoscale solidification of an Al-9.68 at% Ag sample, with time shown in seconds passed since the start of solidification within the viewing window. (d-i) Additional frames for a region of interest in the middle right of the full sample. Lighter regions are Al-rich, whereas darker regions are Ag-rich.

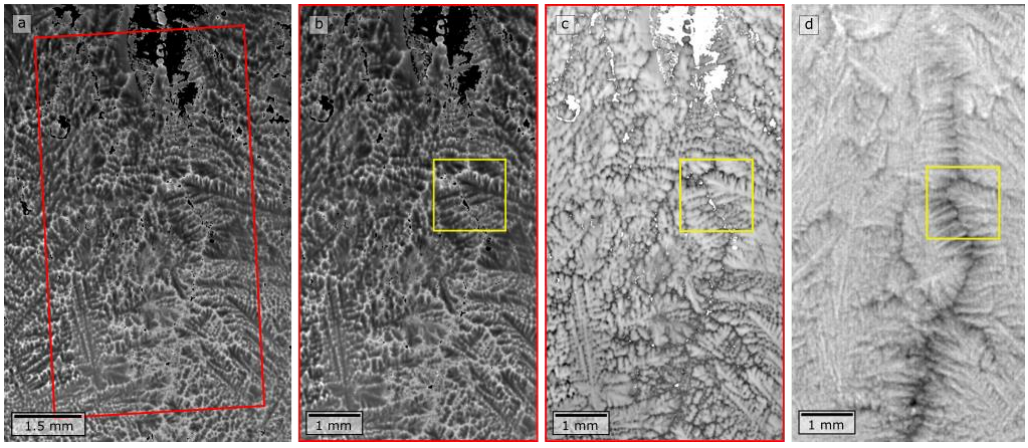

Figure 32.3: (a) Post-solidification BSE image montage with the area of the sample analyzed through in situ x-radiography indicated by the red overlay. (b) BSE montage rotated and cropped to the x-radiography analysis area with the yellow overlay corresponding to the region of interest in Figure 32.2 d-i. (c) BSE montage with grayscale values inverted to facilitate visual comparison to x-radiography with the region of interest once again indicated by the yellow overlay. (d) X-radiograph of the post-solidification sample (939 seconds after the start of solidification). Yellow overlay corresponds to the same region of interest as in b and c.

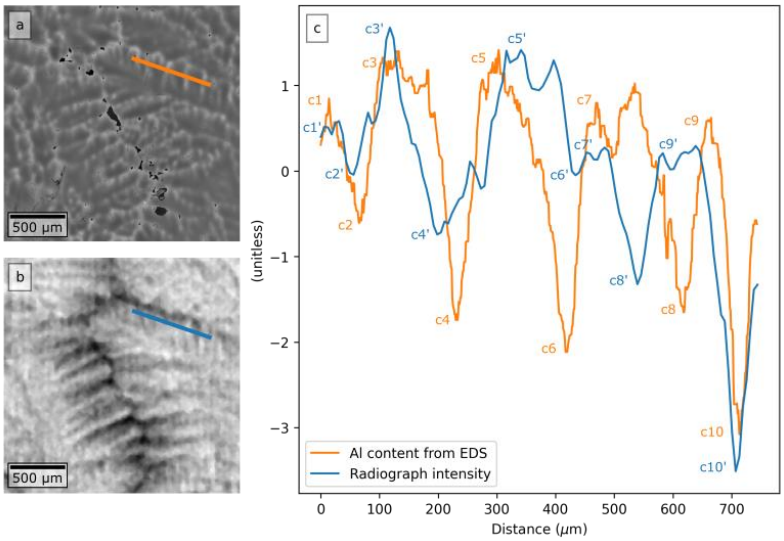

Figure 32.4: (a) BSE image of an Al-Ag sample showing the position of an EDS line scan measuring the Al content. (b) X-radiograph of the same sample region. (c) Al content from the EDS line scan (orange) and the transmitted x-ray intensity (blue), collected across the length of the lines in a and b respectively. Each dataset is standardized to a unitless range for comparison. EDS features annotated as c1-10 correlate to x-radiography features annotated as c1'-10' respectively.

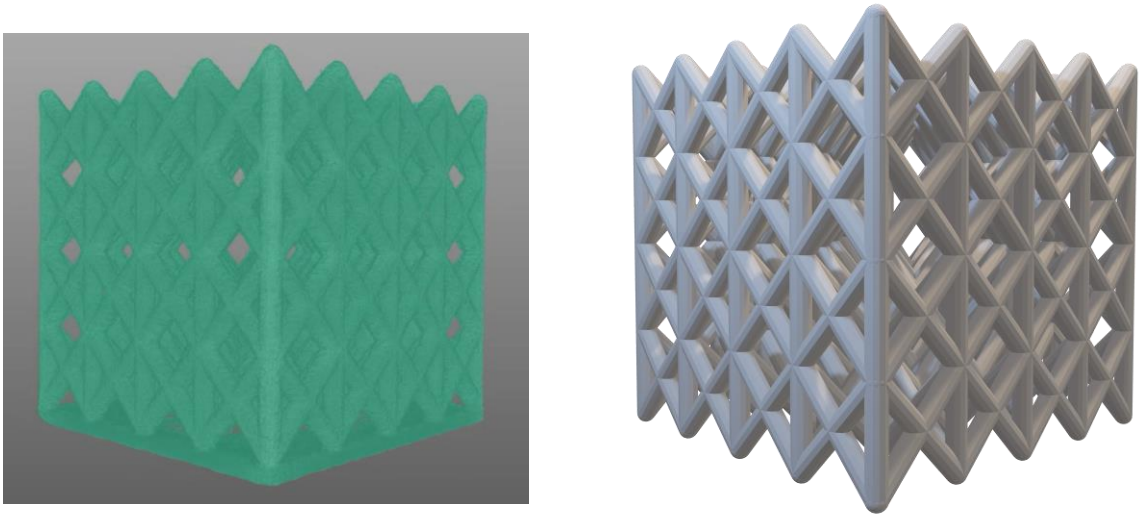

(a) (b)

Figure 32.5: (a) Reconstructed CT analysis of AM-built lattice structures captured with the Zeiss Xradia Versa 520 Micro-CT instrument at Mines. (b) Build model used to additively manufacture the sample is shown in (a).

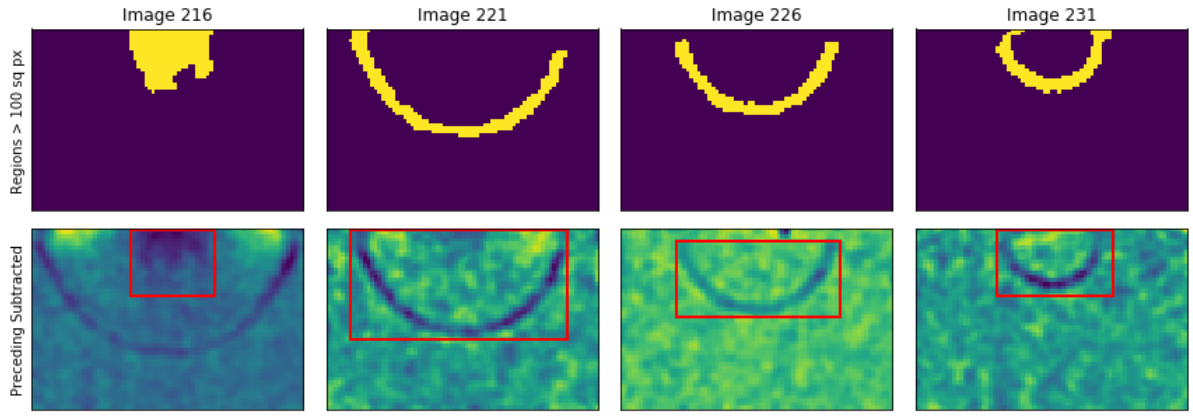

Figure 32.6: Results of the process to automate the detection of the solid-liquid interface in additive manufacturing simulator experiments performed at the Advanced Photon Source at Argonne National Laboratory.

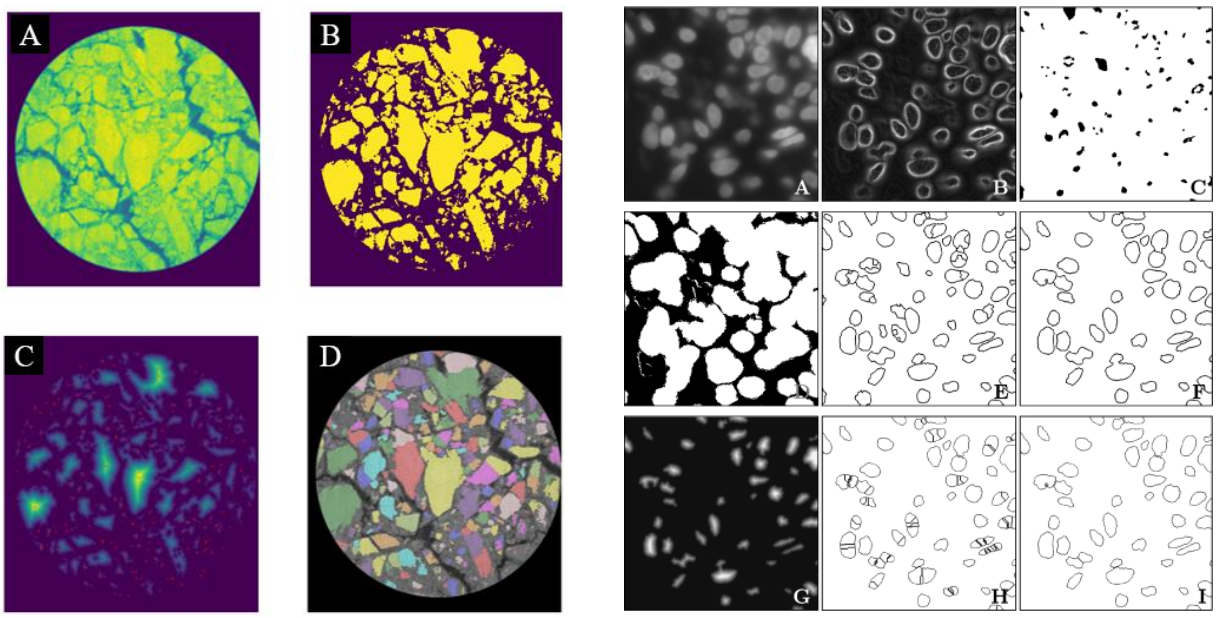

(a) (b)

Figure 32.7: (a) Current method of segmenting mock HE crystals from surrounding binder. A: Original image. B: Threshold at manually chosen value. C: Create distance map and identify local maxima. D: Watershed segmentation with local maxima as seeds. (b) Method of C. Wälhby et al. [32.10] for segmentation that combines intensity, edge, and shape information. A: Original fluorescence microscopy image slice of a tumor. B: Gradient of A. C: Foreground seeds from local maxima. D: Background seeds from local maxima of B (with removal of small components). E: Seeded watershed segmentation. F: Merging of seeded objects based on edge strength. G: Distance map of E. H: Watershed segmentation of distance transform before merging. I: Final segmentation result based on intensity, edge, and shape information.